

Article

Oil-in-Water Self-Assembled Synthesis of Ag@AgCl Nano-Particles on Flower-like Bi₂O₂CO₃ with Enhanced Visible-Light-Driven Photocatalytic Activity

Shuanglong Lin ¹, Li Liu ^{1,2}, Yinghua Liang ², Wenquan Cui ^{2,*} and Zisheng Zhang ^{1,3,*}

¹ School of Chemical Engineering and Technology, Tianjin University, Tianjin 300072, China; linshuanglong15@126.com (S.L.); chemll@126.com (L.L.)

² College of Chemical Engineering, Hebei Key Laboratory for Environment Photocatalytic and Electrocatalytic Materials, North China University of Science and Technology, Tangshan 063009, China; liangyh@ncst.edu.com

³ Department of Chemical and Biological Engineering, University of Ottawa, Ottawa, ON K1N 6N5, Canada

* Correspondence: wkcui@163.com (W.C.); Jason.zhang@uottawa.ca (Z.Z.);
Tel.: +86-187-1609-1609 (W.C.); +86-188-0222-5968 (Z.Z.)

Academic Editor: Erik Reimhult

Received: 9 May 2016; Accepted: 12 June 2016; Published: 17 June 2016

Abstract: In this work, a series of novel flower-like Ag@AgCl/Bi₂O₂CO₃ were prepared by simple and feasible oil-in-water self-assembly processes. The phase structures of as-prepared samples were examined by X-ray diffraction (XRD), Scanning electron microscopy (SEM), Transmission electron microscopy (TEM), UV-vis diffuse reflectance spectroscopy (DRS), X-ray fluorescence spectrometer (XRF), *etc.* The characterization results indicated that the presence of Ag@AgCl did not affect the crystal structure, but exerted a great influence on the photocatalytic activity of Bi₂O₂CO₃ and enhanced the absorption band of pure Bi₂O₂CO₃. The photocatalytic activities of the Ag@AgCl/Bi₂O₂CO₃ samples were determined by photocatalytic degradation of methylene blue (MB) under visible light irradiation. The Ag@AgCl (10 wt %)/Bi₂O₂CO₃ composite showed the highest photocatalytic activity, degrading 97.9% MB after irradiation for 20 min, which is over 1.64 and 3.66 times faster than that of pure Ag@AgCl (calculated based on the equivalent Ag@AgCl content in Ag@AgCl (10 wt %)/Bi₂O₂CO₃) and pure Bi₂O₂CO₃, respectively. Bisphenol A (BPA) was also degraded to further prove the degradation ability of Ag@AgCl/Bi₂O₂CO₃. Photocurrent studies indicated that the recombination of photo-generated electron-hole pairs was decreased effectively due to the formation of heterojunctions between flower-like Bi₂O₂CO₃ and Ag@AgCl nanoparticles. Trapping experiments indicated that O₂^{•−}, h⁺ and Cl[•] acted as the main reactive species for MB degradation in the present photocatalytic system. Furthermore, the cycling experiments revealed the good stability of Ag@AgCl/Bi₂O₂CO₃ composites. Based on the above, a photocatalytic mechanism for the degradation of organic compounds over Ag@AgCl/Bi₂O₂CO₃ was proposed.

Keywords: nanoparticles; oil-in-water self-assembly; Ag@AgCl/Bi₂O₂CO₃; photocatalysis; methylene blue degradation

1. Introduction

Bismuth-based oxides with 3D hierarchical architectures have recently attracted much attention among various semiconductor photocatalysts such as Bi₂O₃ [1], Bi₂WO₆ [2], Bi₂MoO₆ [3], BiOCl [4] and Bi₂O₂CO₃ [5] because of their valence bands hybridized by O 2p and Bi 6s [6]. Among these compounds, Bismuth subcarbonate (Bi₂O₂CO₃), as a typical member of the Aurivillius-related oxide

family, is constructed by $(\text{Bi}_2\text{O}_2)^{2+}$ slabs interleaved by CO_3^{2-} layers [7]. Very recently, it has been found to exhibit a promising antibacterial performance and a photocatalytic activity capable of degrading pollutants [8–13].

Up until now, various morphologies of $\text{Bi}_2\text{O}_2\text{CO}_3$ have been obtained. For instance, Zheng and co-workers have synthesized flower-like, sponge-like, porous spheres and plate-like $\text{Bi}_2\text{O}_2\text{CO}_3$ samples, and have investigated their photocatalytic properties with regards to the degradation of organic pollutants under solar light [14]. They found that the flower-like $\text{Bi}_2\text{O}_2\text{CO}_3$ assembled by nanoflakes showed the best photocatalytic performance in which over 95% of the RhB solution (10–5 M) was degraded after approximately 50 min. The $\text{Bi}_2\text{O}_2\text{CO}_3$ microflowers synthesized by Cheng *et al.* could degrade 83% methyl orange (MO) within 150 min, which was much higher than that of commercial $\text{Bi}_2\text{O}_2\text{CO}_3$ [15].

However, $\text{Bi}_2\text{O}_2\text{CO}_3$ with the wide band gap can only absorb UV light (less than 5% of the solar light spectrum), restricting its practical application under solar light [16,17]. On the other hand, the photocatalytic efficiency of a photocatalyst is also usually limited by its ability to separate and/or combine photo-generated electron–hole pairs. Therefore, it is necessary to develop an effective strategy to improve charge separation efficiency and to enhance the visible light responsive activity of photocatalysts.

To address this issue, an enormous amount of research effort has been focused on combining $\text{Bi}_2\text{O}_2\text{CO}_3$ with lower band semiconductors such as MoS_2 [18], $\text{g-C}_3\text{N}_4$ [19], Fe_2O_3 [20], *etc.* to extend the absorption range. Previous reports revealed that silver@silver halide [21] (Ag@AgX ($X = \text{Cl}, \text{Br}$ and I)) photocatalysts possess excellent visible light driven photocatalytic degradation efficiencies for organic pollutants and disinfection capabilities due to the localized surface plasmon resonance (SPR) effect exhibited by Ag nanoparticles (NPs). The surface plasmon resonance (SPR) of Ag nanoparticles has been used for photocatalysts due to its excellent absorption in the visible light region. Ag/AgX ($X = \text{Cl}, \text{Br}$ and I) have become the focus of the photocatalysts due to their extraordinary plasma effect for specific applications, such as visible light harvesting for bacteria destruction and the degradation of organic pollutants in water [22,23]. Importantly, recent works have led to the development of Ag@AgX -based composite photocatalysts with the advantages of efficient visible light absorption, low cost, and relative stability. For example, it has been reported that $\text{Ag@AgCl}/\text{WO}_3$, $\text{Ag@AgCl}/\text{MCM-41}$, $\text{Ag@AgI}/\text{Al}_2\text{O}_3$, $\text{Ag@AgCl}/\text{GO}$, and AgI/TiO_2 showed enhanced visible light photocatalytic degradation and disinfection.

To the best of our knowledge, there is no work focused on the preparation of and the photocatalytic activity of Ag@AgCl modified $\text{Bi}_2\text{O}_2\text{CO}_3$ photocatalysts. Based on previous studies, $\text{Bi}_2\text{O}_2\text{CO}_3$ modified with Ag@AgCl to form $\text{Ag@AgCl}/\text{Bi}_2\text{O}_2\text{CO}_3$ heterojunctions may improve visible light activated photocatalytic activity. On one hand, 3D hierarchical architectures could make pure $\text{Bi}_2\text{O}_2\text{CO}_3$ visible light-active through surface scattering and reflecting (SSR) effects [24]. On the other hand, the surface plasmon resonance effects (SPR effects) of Ag@AgCl decorated on the $\text{Bi}_2\text{O}_2\text{CO}_3$ surface could further strengthen the visible light absorption of 3D $\text{Bi}_2\text{O}_2\text{CO}_3$ hierarchical microspheres [25]. In this article, Ag@AgCl -decorated $\text{Bi}_2\text{O}_2\text{CO}_3$ (hereafter designated as NPs $\text{Ag@AgCl}/\text{Bi}_2\text{O}_2\text{CO}_3$) was successfully synthesized via a multistep route, in which a hydrothermal precipitation was employed to synthesize flower-like $\text{Bi}_2\text{O}_2\text{CO}_3$. An oil-in-water self-assembly synthesis was used to deposit NPs Ag@AgCl on Bi_2WO_6 . The characterization and a possible photocatalytic mechanism for the $\text{Ag@AgCl}/\text{Bi}_2\text{O}_2\text{CO}_3$ composites were discussed in detail.

2. Experimental

2.1. Photocatalyst Synthesis

All chemical reagents purchased were of analytical grade and used without further purification. The flower-like $\text{Bi}_2\text{O}_2\text{CO}_3$ precursor was synthesized by a hydrothermal method. In a typical procedure to prepare flower-like $\text{Bi}_2\text{O}_2\text{CO}_3$ precursor, 3 mmol of $\text{Bi}(\text{NO}_3)_3 \cdot 5\text{H}_2\text{O}$ were dissolved in 20 mL of

1 M HNO_3 , and then 2 mmol of citric acid were introduced to the solution. After being magnetically stirred for 10 min, the pH of the solution was adjusted to 4–4.2 with the addition of NaOH solution under vigorous stirring. The white precursor that formed was transferred to a Teflon-lined stainless steel autoclave and maintained at 160 °C for 24 h. After cooling the hydrothermal system to room temperature, the flower-like $\text{Bi}_2\text{O}_2\text{CO}_3$ precursor was separated by a centrifugation process, washed several times with distilled water and ethanol, and dried under vacuum at 80 °C for 8 h.

The $\text{Ag@AgCl/Bi}_2\text{O}_2\text{CO}_3$ composite was prepared by a novel oil-in-water self-assembly method under dark conditions (As shown in Figure 1). Typically, 0.5g $\text{Bi}_2\text{O}_2\text{CO}_3$ powder and AgNO_3 were dissolved into 20 mL deionized water and a certain amount ($n_{\text{AgNO}_3}:n_{\text{CTAC}} = 1:1.5$) of Cetyl trimethyl ammonium chloride (CTAC)/carbon tetrachloride solution (40 mL) was added dropwise at room temperature under vigorous magnetic stirring over 20 min. After the CTAC addition, the reaction mixture was magnetically stirred for another 20 min. The resulting suspension was then filtered and washed with deionized water and ethanol, respectively. The obtained $\text{AgCl/Bi}_2\text{O}_2\text{CO}_3$ powder was dispersed in 30 mL distilled water, and irradiated with a 250 W metal halide lamp (Philips), equipped with wavelength cutoff filters for $\lambda \geq 420$ nm. The resulting sample ($\text{Ag@AgCl/Bi}_2\text{O}_2\text{CO}_3$) was washed with distilled water and anhydrous ethanol to remove the surfactant, and the final products (hereafter designated $\text{Ag@AgCl/Bi}_2\text{O}_2\text{CO}_3$) were dried at 80 °C for 8 h in the dark. $\text{Ag@AgCl/Bi}_2\text{O}_2\text{CO}_3$ composites with different molar ratios of Ag@AgCl to $\text{Bi}_2\text{O}_2\text{CO}_3$ were prepared according to the typical procedure described above.

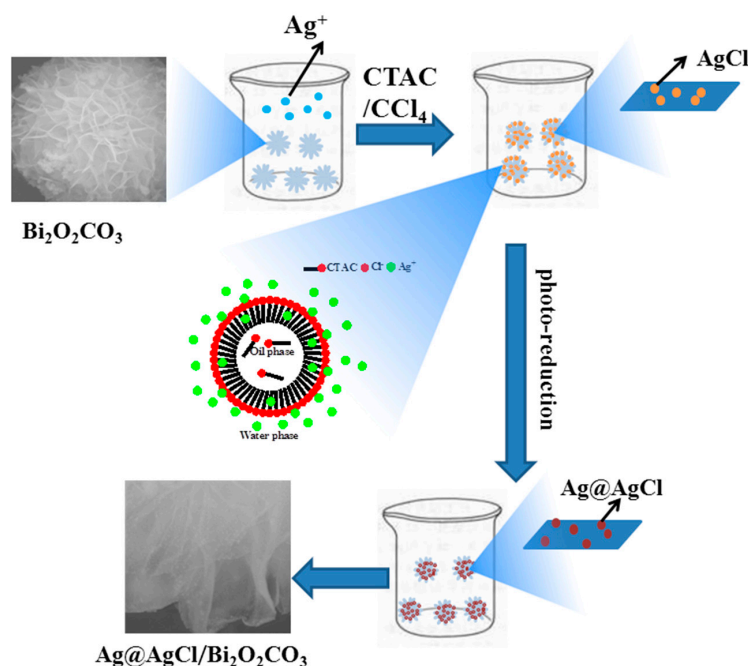


Figure 1. Schematic illustration for the preparation of $\text{Ag@AgCl/Bi}_2\text{O}_2\text{CO}_3$.

For comparison, an $\text{Ag@AgCl/Bi}_2\text{O}_2\text{CO}_3$ sample was prepared via a precipitation method with $\text{Bi}_2\text{O}_2\text{CO}_3$ powder, NaOH, AgNO_3 and CTAC. The as-prepared catalyst was denoted as P- $\text{Ag@AgCl/Bi}_2\text{O}_2\text{CO}_3$.

Pure Ag@AgCl was synthesized similarly using an oil-in-water self-assembly method with AgNO_3 , and CTAC.

2.2. Photocatalyst Characterization

The crystal structures and phase data for the prepared samples were determined by X-ray diffractometry (XRD) using a Rigaku D/MAX2500 PC diffractometer (D/MAX2500 PC,

Rigaku Corporation, Tokyo, Japan) with Cu K α radiation, with an operating voltage of 40 kV and an operating current of 100 mA. The morphologies of the samples were investigated with a scanning electron microscope (SEM) (Hitachi, Chiyoda, Japan, s-4800) and energy dispersive X-ray spectroscopy (EDX), as well as by transmission electron microscopy (TEM) (JEOL Ltd., Akishima, Japan, JEM-2010). UV-visible light (UV-vis) diffuse reflectance spectra were recorded on a UV-vis spectrometer (UV-1901, Puxi, Beijing, China). The chemical compositions of the samples were tested by an X-ray fluorescence spectrometer (XRF, Rigaku, Tokyo, Japan, ZSX PromuII). Surface areas of the samples were determined by the Brunauer-Emmett-Teller (BET) method based on the adsorption and desorption isotherms of N₂ collected on a Quantachrome Nova 4200e automatic analyzer (Monorosb, Quantachrome, Boynton Beach, FL, USA). The photoluminescence of the powdered samples was measured by a spectrofluorometer (Hitachi, f7000). Electrochemical and photoelectrochemical measurements were performed in a constructed three electrode quartz cell system. A Pt sheet was used as a counter electrode and Hg/Hg₂Cl₂/sat. KCl was used as a reference electrode, while the thin film on indium-tin oxide (ITO) was used as the working electrode for investigation. The photoelectrochemical experimental results were recorded with a CHI 660B electrochemical system.

2.3. Photocatalytic Activity

The photocatalytic activities of Ag@AgCl/Bi₂O₂CO₃ composites were evaluated by the degradation of methylene blue (MB) under irradiation of visible light. For the first series of tests, a 250 W halide lamp (Royal Philips, Amsterdam, The Netherlands) with a 420 nm cutoff filter was used at a distance of 10 cm from the top of an unsealed beaker. In a second series of tests, a glass reactor with circulating water flowing outside to control the temperature to 25 ± 2 °C was employed. For each test, 0.4 g catalyst powder was added to 100 mL 10 mg/L MB solution. Prior to irradiation, the test solution was stirred in the dark for 30 min. During irradiation, a 3 mL aliquot of the reaction suspension was withdrawn every 5 min and centrifuged at 10,000 rpm for 6 min to remove the particles. The collected supernatant solutions were then analyzed by a UV-vis spectrophotometer.

The degradation efficiency (%) was calculated as follows:

$$\text{Degradation}(\%) = \frac{C_0 - C}{C_0} \times 100\% \quad (1)$$

where C_0 is the initial concentration of MB; and C is the concentration of MB at time t .

Photocatalytic activities while degrading MB in the dark in the presence of the photocatalyst and under visible-light irradiation in the absence of the photocatalyst were also evaluated.

Additionally, the degradation procedure of Bisphenol A (BPA) was the same as that of MB.

3. Result and Discussion

3.1. Catalyst Characterization

The XRD study was carried out to confirm the crystalline structure of the as-prepared Ag@AgCl/Bi₂O₂CO₃ composites. Figure 2 shows the XRD patterns of Ag@AgCl, Bi₂O₂CO₃ and Ag@AgCl/Bi₂O₂CO₃ heterojunctions with different Ag@AgCl contents. The Ag@AgCl was found to be mainly composed of the chlorargyrite AgCl phase. The XRD peaks of AgCl were in good agreement with the cubic crystalline phase of AgCl (JCPDS 31-1238), revealing three distinct diffraction peaks at 27.8°, 32.2°, 46.2° and 54.8°, which can be indexed to the (111), (200), (220) and (311) diffraction planes of AgCl, respectively, while the peaks at 38.1° (111) can be attributed to the small quantity of Ag (JCPDS 04-0783) that formed. The pure Bi₂O₂CO₃ and Ag@AgCl/Bi₂O₂CO₃ both have serious distinct diffraction peaks at the same degree, which can be indexed for bismuth subcarbonate of JCPDS 41-1488. The diffraction peaks observed appearing at 2 θ values of 23.9°, 30.3°, 32.7°, 47.0°, 52.2° and 53.4° were assigned to (011), (013), (110), (020), (116) and (121) crystal planes of rhombic Bi₂O₂CO₃,

respectively. The presence of Ag@AgCl in Ag@AgCl/Bi₂O₂CO₃ composites was confirmed by the following SEM and TEM images.

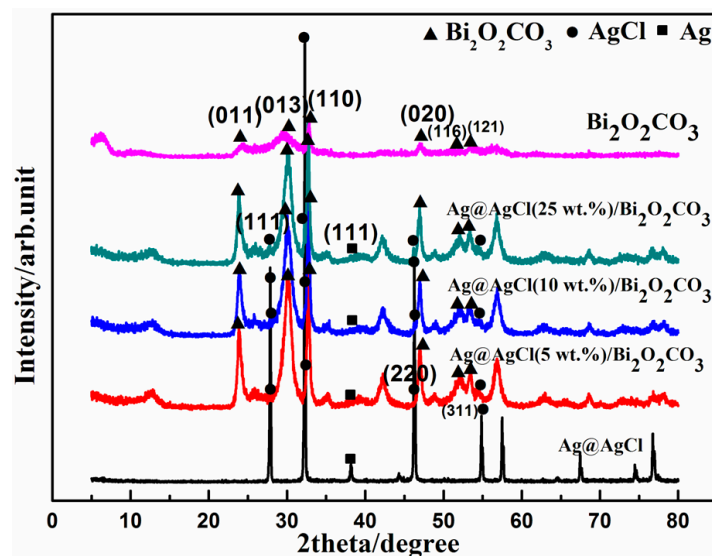


Figure 2. XRD pattern of Ag@AgCl, Bi₂O₂CO₃ and Ag@AgCl/Bi₂O₂CO₃ composites.

The morphology of the Ag@AgCl/Bi₂O₂CO₃ composite was studied by SEM, TEM and HRTEM. It can be observed from Figure 3a that the diameter of a flower-like Bi₂O₂CO₃ microsphere is 1–2 μm, built from two-dimensional nanoplates with a smooth surface. The as-synthesized Ag@AgCl nanoparticles have a nearly spherical shape with a diameter of 80–100 nm (Figure 3b). Figure 3c shows that some Ag@AgCl particles of the size 0.3–0.5 μm are randomly attached to the surface of Bi₂O₂CO₃ microspheres via a precipitation method. However, the sample containing Ag@AgCl deposited onto Bi₂O₂CO₃ prepared by a self-assembly method is shown in Figure 3d. The shape of Bi₂O₂CO₃ did not change upon NPs Ag@AgCl-loading, which indicates that the NPs Ag@AgCl deposition process does not damage its flower-like structure. In addition, Ag@AgCl-loading could very well promote the scattering of Ag@AgCl, and reduce its grain size. From Figure 3d, some spherical particles with a size range of 5 to 20 nm were observed to be uniformly deposited on the surface of Bi₂O₂CO₃, indicating the increased surface roughness of the flower-like structure [26]. The BET results revealed that the specific surface area of the Ag@AgCl (25 wt %)/Bi₂O₂CO₃ (24.23 m²·g⁻¹) nano-composite was larger than that of pure Bi₂O₂CO₃ (13.61 m²·g⁻¹) (as shown in Table 1). The light absorption was considered to be enhanced due to the increased light scattering. Figure 3e shows the TEM image of flower-like microstructures. According to the TEM image in Figure 3f, Ag@AgCl nanoparticles with a size of about 10 nm were attached to the flower-like nanostructures of Bi₂O₂CO₃. It can be seen from the HRTEM images (Figure 3g), that the clear lattice fringe indicates the high-crystallinity of the composite. The lattice fringes of Ag, AgCl and Bi₂O₂CO₃ coexist in the Ag@AgCl/Bi₂O₂CO₃ composite. The measured interplanar spacings of 0.24 nm, 0.28 nm and 0.27 nm correspond to the (111) plane of Ag, the (200) plane of AgCl and the (110) plane of Bi₂O₂CO₃. This revealed that the nanoparticles formed on Bi₂O₂CO₃ were Ag@AgCl. The SAED pattern collected from Ag@AgCl/Bi₂O₂CO₃ is shown in Figure 3h, where polycrystalline diffraction rings can be observed. The characteristic peak of Ag@AgCl/Bi₂O₂CO₃ can be obviously observed in EDX (Figure 3i). This further proves the formation of Ag@AgCl on Bi₂O₂CO₃. In addition, the elemental compositions of the composite nanoparticles were further analyzed by XRF. The results are shown in Table 2, and the atomic ratio of Ag to Cl was found to be 1.49:1, indicating the presence of Ag in the Ag@AgCl nanojunction system. Based on the XRF results, the atomic ratio of Bi to C to O was found to be 1.9:1:5.5, which was less than the theoretical ratio of 2:1:5 expected from Bi₂O₂CO₃. Since the percentages of O and C were higher in

the experimental sample than in the theoretical ratio for $\text{Bi}_2\text{O}_2\text{CO}_3$, H_2O and/or C were thought to possibly be present in the prepared $\text{Ag@AgCl}/\text{Bi}_2\text{O}_2\text{CO}_3$ composite.

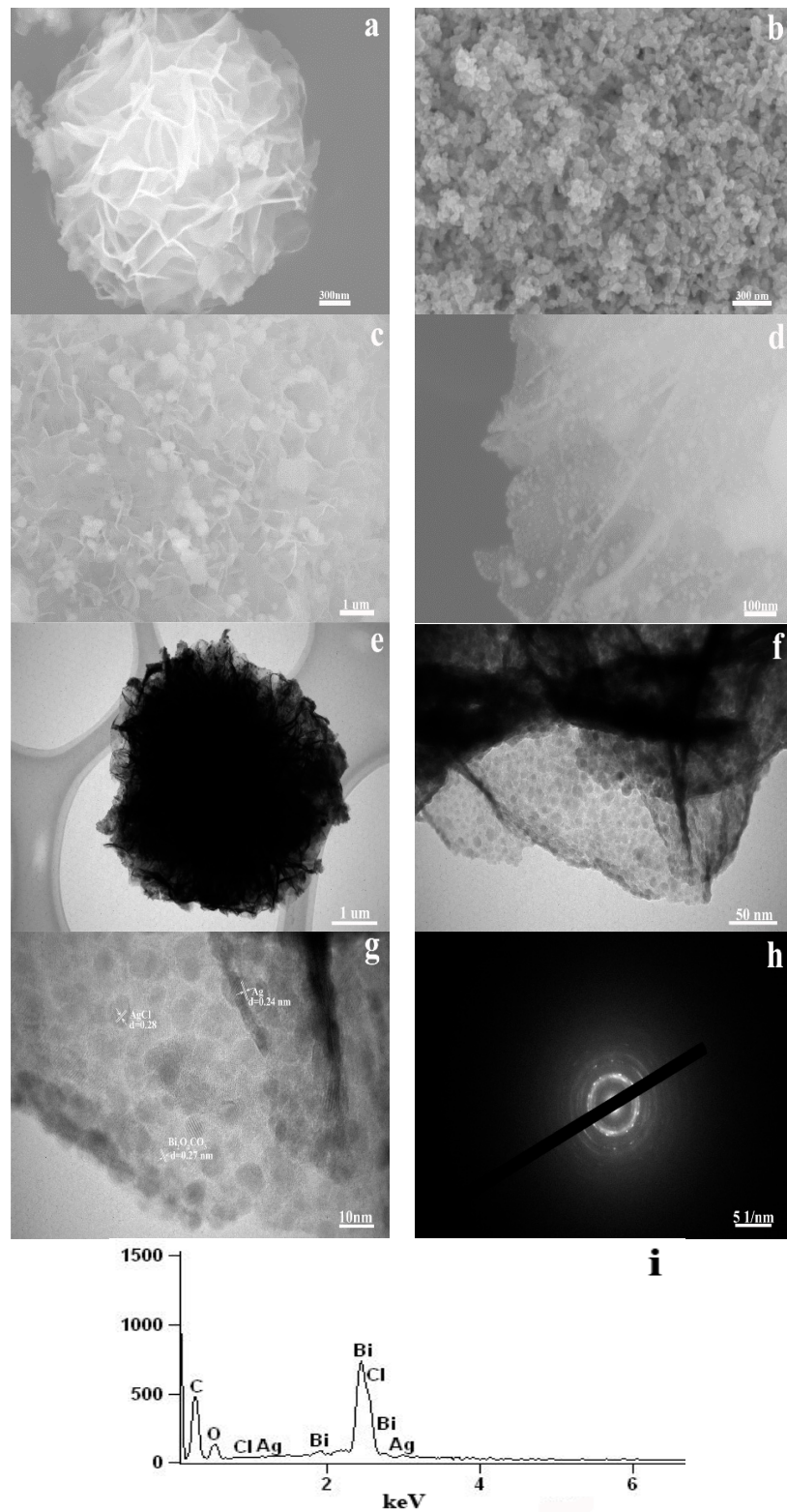


Figure 3. SEM images of: (a) $\text{Bi}_2\text{O}_2\text{CO}_3$; (b) Ag@AgCl ; (c) $\text{P-Ag@AgCl}/\text{Bi}_2\text{O}_2\text{CO}_3$; and (d) $\text{Ag@AgCl}/\text{Bi}_2\text{O}_2\text{CO}_3$. TEM images of (e,f) $\text{Ag@AgCl}/\text{Bi}_2\text{O}_2\text{CO}_3$. HRTEM and SAED images of (g,h) $\text{Ag@AgCl}/\text{Bi}_2\text{O}_2\text{CO}_3$. EDX spectrum of (i) $\text{Ag@AgCl}/\text{Bi}_2\text{O}_2\text{CO}_3$ samples.

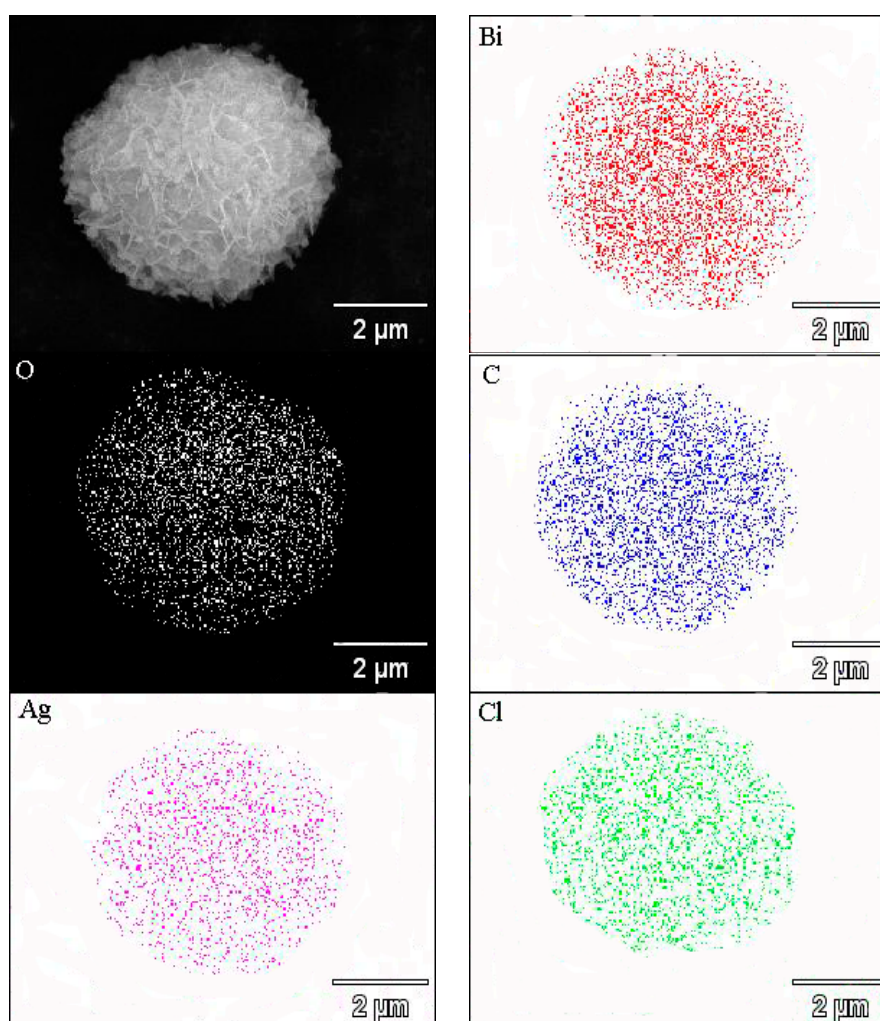
Table 1. Specific surface area of Ag@AgCl/Bi₂WO₆ composite catalysts.

Photocatalysts	Bi ₂ O ₂ CO ₃	Ag@AgCl (5 wt %)/ Bi ₂ O ₂ CO ₃	Ag@AgCl (20 wt %)/ Bi ₂ O ₂ CO ₃	Ag@AgCl (25 wt %)/ Bi ₂ O ₂ CO ₃
Surface area (m ² ·g ⁻¹)	13.61	14.23	22.07	24.23

Table 2. The major elemental content of photocatalysts.

Major Element	Ag	Cl	Bi	C	O
Ag@AgCl (10 wt %)/Bi ₂ O ₂ CO ₃ (content, mass %)	7.55	1.68	67.28	2.08	16.81

The EDX elemental mapping of the Ag@AgCl/Bi₂O₂CO₃ composites (Figure 4) displays the even distribution of the elements Ag, Cl, Bi, C and O on Ag@AgCl/Bi₂O₂CO₃. The elements of Ag and Cl are from Ag@AgCl. Bi, C and O are from Bi₂O₂CO₃. The results further indicate the chemical uniformity within individual particles, which clearly confirms that the Ag@AgCl NPs were uniformly distributed on the surface of the Bi₂O₂CO₃ flower-like microspheres. All of the above structure characterizations indicate that a promising Ag@AgCl/Bi₂O₂CO₃ photocatalyst with well-designed architecture was constructed.

**Figure 4.** SEM image and EDX elemental maps of spherical structure of Ag@AgCl/Bi₂O₂CO₃ composite photocatalyst.

It is well known that the UV-vis absorption edge is related to the energy band of the semiconductor catalyst, depending on its electronic structure [18]. The optical absorption property of Ag@AgCl/Bi₂O₂CO₃ composites was analyzed. Figure 5 shows the UV-vis diffuse reflectance spectra of Ag@AgCl, Bi₂O₂CO₃ and Ag@AgCl/Bi₂O₂CO₃ composites. Clearly, it can be seen that pure Bi₂O₂CO₃ boasted a weak visible light response with an absorption band edge of about 365 nm. After Ag@AgCl was introduced, the ability of light absorption for Bi₂O₂CO₃ was drastically enhanced due to the surface plasmonic resonance (SPR) of Ag nanoparticles on Ag@AgCl in visible light. Accordingly, with the increase in Ag@AgCl content, the differences in optical adsorption agree well with the colors, changing from white to dark-gray. Additionally, a slight redshift in the absorbance region was observed with the increase in Ag@AgCl content, which might be caused by a possible charge-transfer transition at the interface between Ag@AgCl and Bi₂O₂CO₃, due to the presence of Ag@AgCl [27]. These results also indicate that Ag@AgCl exists on the surface of Bi₂O₂CO₃ and that the Ag@AgCl/Bi₂O₂CO₃ photocatalysts are more effective at degrading organic dyes under light irradiation. On the other hand, for a crystalline semiconductor, the optical absorption near band edge follows the following formula [19]:

$$\alpha h\nu = A (h\nu - E_g)^{n/2} \quad (2)$$

where α , h , ν , E_g , and A are the absorption coefficient, Plank constant, light frequency, band gap, and a constant, respectively [28]. Among them, n is 1 for a direct transition and 4 for an indirect transition. Bi₂O₂CO₃ processes indirect transition band gaps [29,30], and so in this case, the value of n is equal to 4. The E_g value can be estimated by extrapolating the straight portion of the $(\alpha h\nu)^{1/2} - (h\nu)$ plot to the $\alpha = 0$ point, where the band gap of Bi₂O₂CO₃ is 3.4 eV (see inset of Figure 5). As a consequence, the Ag@AgCl/Bi₂O₂CO₃ sample can more easily produce electron-hole pairs under the same UV light irradiation and display higher photocatalytic activities.

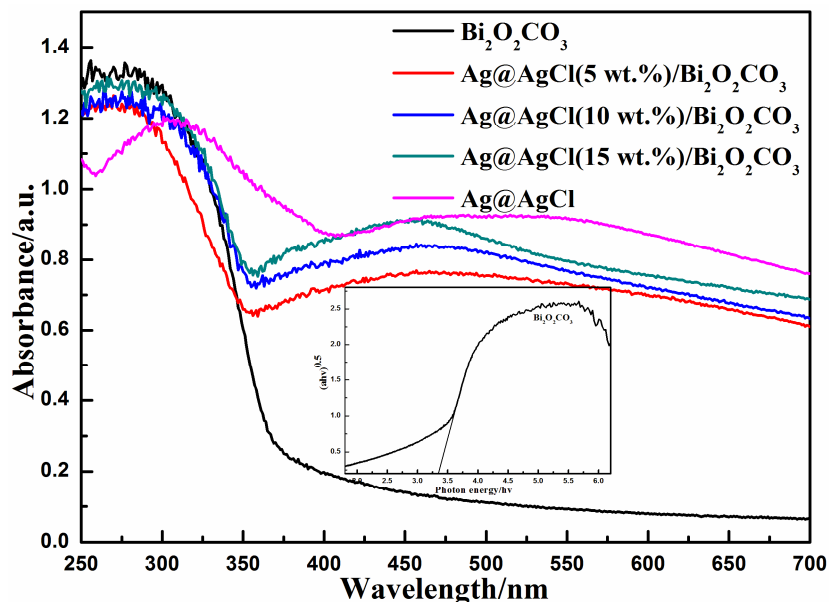


Figure 5. UV-vis diffuse reflectance spectrum (DRS) of as-prepared Bi₂O₂CO₃, Ag@AgCl and a series of Ag@AgCl/Bi₂O₂CO₃ composites (inset: band gap determination of pure Bi₂O₂CO₃ samples).

In order to further determine the chemical state of elements present in the synthesized samples, Ag@AgCl/Bi₂O₂CO₃ samples were analyzed by X-ray photoelectron spectroscopy (XPS), and the results are shown in Figure 6. Figure 6a shows wide-scan XPS spectra of Ag@AgCl/Bi₂O₂CO₃ samples. As shown, the presences of bismuth (Bi 4f, Bi 4d, Bi 4p and Bi 5d), oxygen (O 1s), carbon (C 1s), silver (Ag 3d) and chlorine (Cl 2p) in the Ag@AgCl/Bi₂O₂CO₃ sample were confirmed. Furthermore,

high-resolution XPS spectra of Ag in the synthesized sample are shown in Figure 6b. As shown in Figure 6b, for the Ag@AgCl/Bi₂O₂CO₃ sample, the peaks at 373.13 and 366.85 eV correspond to Ag 3d_{3/2} and Ag 3d_{5/2} respectively. It is noted that the Ag 3d_{3/2} peak can be further divided into two separate peaks at 374.46 and 373.01 eV, while the Ag 3d_{5/2} peak can also be divided into two separate peaks at 368.17 and 366.78 eV. The peaks at 366.78 and 373.01 eV can be attributed to Ag⁺ of AgCl, while the peaks at 374.46 and 368.17 eV can be assigned to metallic Ag [31]. The results of XPS analysis confirm the presence of Ag and AgCl in the prepared composite sample.

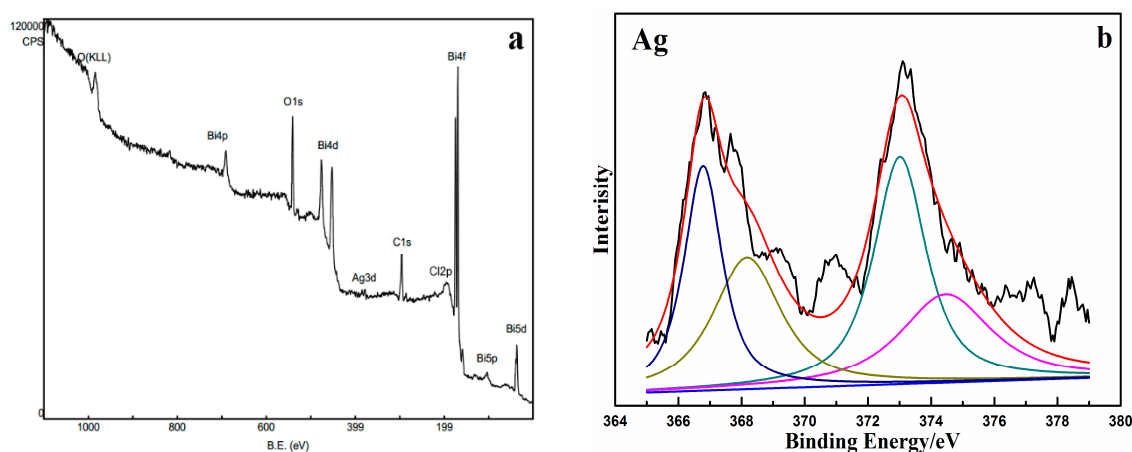


Figure 6. (a) XPS survey spectra of Ag@AgCl/Bi₂O₂CO₃; (b) High-resolution XPS spectra of Ag 3d.

3.2. Photocatalytic Activity

Figure 7 shows the Photocatalytic adsorption (Figure 7a) and degradation (Figure 7b) efficiency changes in the relative concentration of MB (C/C_0) as a function of irradiation time over the Ag@AgCl/Bi₂O₂CO₃ composites with components Ag@AgCl and Bi₂O₂CO₃. Figure 7a shows the adsorption performance of Ag@AgCl, Bi₂O₂CO₃ and Ag@AgCl (10 wt %)/Bi₂O₂CO₃. During the dark period, Ag@AgCl, Bi₂O₂CO₃ and Ag@AgCl (10 wt %)/Bi₂O₂CO₃ removed MB from the solution via adsorption. The adsorption equilibrium was reached between 25 and 30 min for these materials. Upon visible light irradiation, as shown in Figure 7b, blank reaction was also given as controls. The blank experiments which were performed in the absence of a photocatalyst showed no obvious changes in the concentration of MB over 20 min of reaction under visible light irradiation. This verifies that MB is an organic dye which is chemically stable and difficult to decompose. The reaction in dark with Ag@AgCl/Bi₂O₂CO₃ catalysts did not facilitate the degradation of MB. After visible light irradiation for 20 min, the degradation percent of MB by pure Bi₂O₂CO₃ was only 26.77%, which indicates that pure Bi₂O₂CO₃ shows weak activity. The degradation of MB in this situation may be induced by the sensitization effects of dye molecules [32], since Bi₂O₂CO₃ cannot be excited by visible light due to its large band gap (3.4 eV). The Ag@AgCl/Bi₂O₂CO₃ composite displayed the highest activity, and the removal percent of MB reached 97.9% within 20 min, which is over 1.64 and 3.66 times faster than that of pure Ag@AgCl (calculated based on the equivalent Ag@AgCl content in Ag@AgCl (10 wt %)/Bi₂O₂CO₃) and pure Bi₂O₂CO₃, respectively. According to these results, the plasmon resonance of Ag NPs and the charge transfer between nano Ag@AgCl and Bi₂O₂CO₃ leads to a higher photocatalytic activity in Ag@AgCl/Bi₂O₂CO₃ compared to the pure Ag@AgCl and Bi₂O₂CO₃ materials.

The photocatalytic degradation of organic pollutants generally follows pseudo-first-order kinetics. As shown in Figure 8, The k_{app} values of the different samples were calculated in the following order: Ag@AgCl (10 wt %)/Bi₂O₂CO₃ (0.051 min⁻¹) > Ag@AgCl (15 wt %)/Bi₂O₂CO₃ (0.032 min⁻¹) > Ag@AgCl (5 wt %)/Bi₂O₂CO₃ (0.025 min⁻¹) > Ag@AgCl (20 wt %)/Bi₂O₂CO₃ (0.023 min⁻¹) > Ag@AgCl (25 wt %)/Bi₂O₂CO₃ (0.012 min⁻¹). The Ag@AgCl (10 wt %)/Bi₂O₂CO₃ composite

possessed the most optimal activity among all the samples, with an apparent rate constant of 0.051 min^{-1} . The highest activity was obtained for the Ag@AgCl (10 wt %)/ $\text{Bi}_2\text{O}_2\text{CO}_3$ sample, on which more than 97.9% of MB was degraded within 20 min. The photocatalytic performance significantly improved after the introduction of Ag@AgCl and increased with the increase of Ag@AgCl content from 0 to 10 wt %. However, further increase in Ag@AgCl loading resulted in a decrease in photocatalytic activity. Once the loading of Ag@AgCl increases beyond a critical value, the nanoclusters of Ag@AgCl species are thought to agglomerate and shade the active sites on the surface of $\text{Bi}_2\text{O}_2\text{CO}_3$, resulting in lower degradation rates [33]. Simultaneously, this can facilitate the recombination of photoinduced electron-hole pairs. Therefore, suitable Ag@AgCl content was crucial for optimizing the photocatalytic performances of the Ag@AgCl/ $\text{Bi}_2\text{O}_2\text{CO}_3$ composites. The above results imply that significant increases in photoactivity can be ascribed to the synergetic effects of Ag@AgCl and $\text{Bi}_2\text{O}_2\text{CO}_3$ photocatalyst.

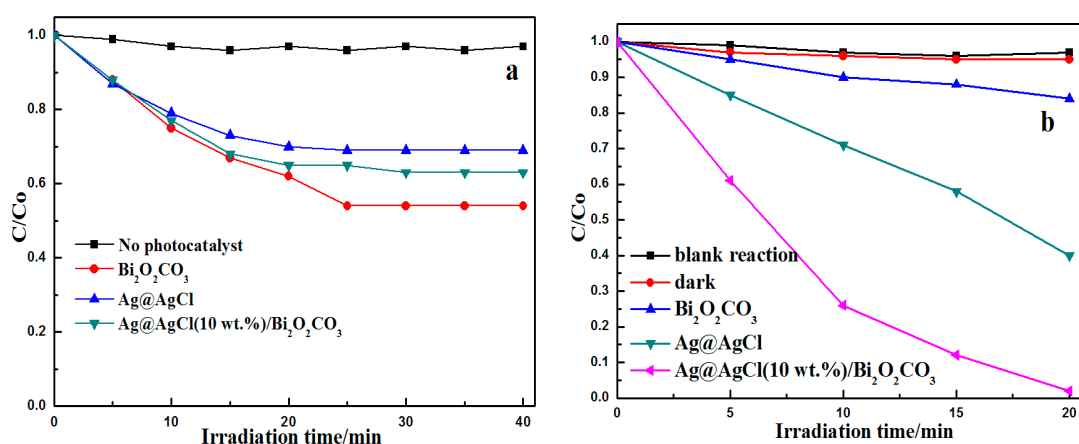


Figure 7. Photocatalytic adsorption (a) and degradation (b) curves of MB over the various samples.

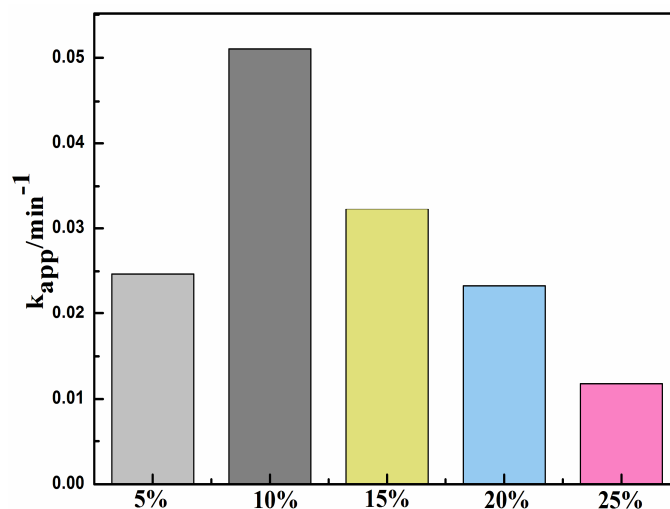


Figure 8. Apparent rate constants for the photocatalytic degradation of MB under the irradiation of visible-light.

To further ascertain the active species in the degradation process and to verify the supposed photocatalytic mechanism, some sacrificial agents such as tert-butyl alcohol (IPA), ethylenediamine tetraacetic acid disodium salt (EDTA-2Na) and nitrogen (N_2) were used as the hydroxyl radical ($-\text{OH}$) scavenger, hole (h^+) scavenger and superoxide radical ($-\text{O}_2^-$) scavenger, respectively [34,35].

As shown in Figure 9, the addition of 1 mM IPA produced an insignificant effect on the degradation rate, demonstrating that -OH radicals play a small role in the photocatalytic degradation of MB. In contrast, the photocatalytic degradation rates of MB decreased significantly in the presence of 1 mM EDTA-2Na and under N_2 -saturated conditions. Compared to the addition of EDTA-2Na, N_2 -saturated conditions have a bigger influence, indicating that h^+ and -O_2^- radicals are the main active species. However, the absolute suppression by IPA, EDTA-2Na and N_2 on photocatalytic activity was not so large, and so it is thought that another important reactive species may affect the observed activity. Considering that the accumulated holes could oxidize Cl^- to Cl° , it was thought that Cl° atoms were the active species that participated in the degradation of MB [36,37]. Accordingly, the active species trapping experiments demonstrated that the h^+ and -O_2^- are the two main active species in the degradation process of MB, which was also in agreement with the supposed photocatalytic mechanism.

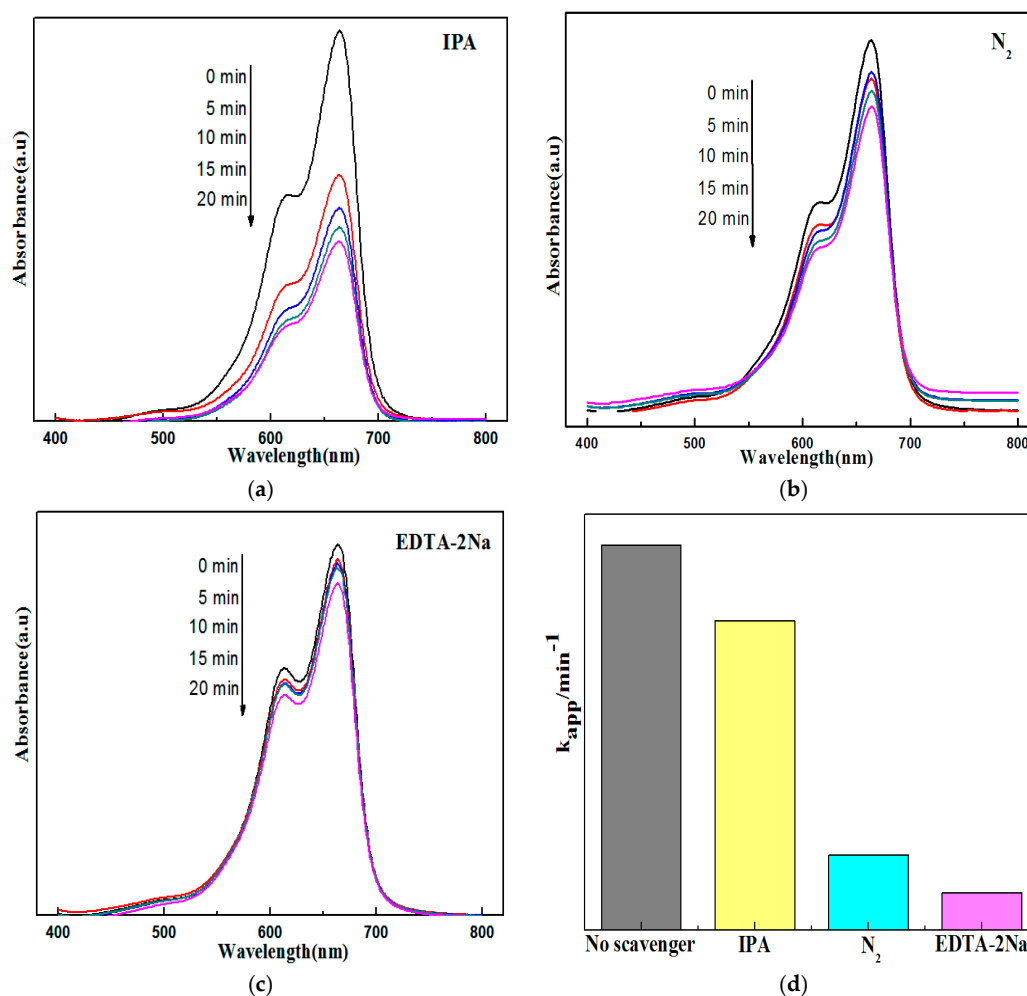


Figure 9. Photocatalytic degradation of MB with $\text{Ag@AgCl/Bi}_2\text{O}_2\text{CO}_3$ in the presence of various scavengers under visible light. (a) IPA; (b) N_2 ; (c) EDTA-2Na; and (d) comparison of the visible-light photocatalytic activity obtained using rate constant k_{app} .

The lifetime of the catalyst is an important parameter of the photocatalytic process. In order to examine the photocatalytic stability of the photocatalyst, the experiment was repeated with the same photocatalyst. The $\text{Ag@AgCl/Bi}_2\text{O}_2\text{CO}_3$ composite was easily recycled by centrifugation and then washed with water and ethanol. After every 20 min of photocatalytic degradation, the separated photocatalysts were washed with deionized water and then with ethanol to dry them. Figure 10 shows the decrease in MB after every run. A high MB photodegradation could be maintained after

five cycling runs with no obvious catalyst deactivation. The slight decrease in photoactivity may be ascribed to the minor loss of catalyst during the recycle experiment [38]. The results confirm that the photoactivity of the Ag@AgCl/Bi₂O₂CO₃ catalyst is stable during the degradation process.

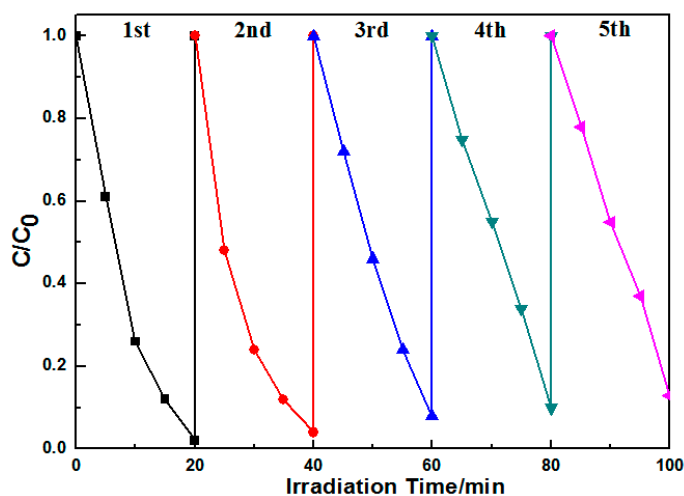


Figure 10. Cycling runs for the photocatalytic degradation of MB in the presence of Ag@AgCl (10 wt %)/Bi₂O₂CO₃ composite under visible light irradiation.

The interfacial charge separation and transfer dynamics of photoelectrons were studied by monitoring their photocurrent-time responses. As shown in Figure 11, the transient photocurrent responses of Bi₂O₂CO₃ and Ag@AgCl/Bi₂O₂CO₃ were tested and showed three on-off cycles of irradiation. The photocurrent responses of as-prepared samples were obtained by the intermittent visible light irradiation of 30 s. The rise and fall of the photocurrent responses are evidently observed for each switch-on and switch-off event, the results demonstrating effective separation of photoinduced electron-hole pairs in Ag@AgCl/Bi₂O₂CO₃ upon exposure to visible light [39]. The results are shown in Figure 11 (the response of the ITO has been deducted as background). It is clear that Ag@AgCl/Bi₂O₂CO₃ shows a much higher photocurrent density than that of pure Bi₂O₂CO₃. The photocurrent result confirms the more efficient separation of photo-generated electron-hole pairs for the Ag@AgCl/Bi₂O₂CO₃ composite than that of pure Bi₂O₂CO₃. This indicates that Ag/AgCl was been effectively combined with Bi₂O₂CO₃, which leads to the efficient separation of the photo-generated electron-hole pairs in Ag@AgCl/Bi₂O₂CO₃.

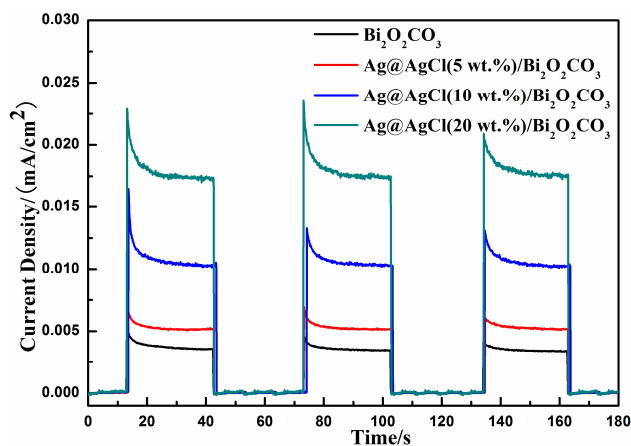


Figure 11. Transient photocurrent response for the pure Bi₂O₂CO₃, Ag@AgCl (5 wt %)/Bi₂O₂CO₃, Ag@AgCl (10 wt %)/Bi₂O₂CO₃ and Ag@AgCl (20 wt %)/Bi₂O₂CO₃.

Electrochemical impedance spectroscopy (EIS) is a very useful tool to characterize charge-carrier migration [40], and was thus used to further confirm the interfacial charge transfer effects of as-prepared composites. Generally, a higher charge mobility results in a smaller EIS arc radius. Figure 12 shows the EIS Nyquist plots of the $\text{Bi}_2\text{O}_2\text{CO}_3$ and $\text{Ag@AgCl}/\text{Bi}_2\text{O}_2\text{CO}_3$ electrodes. Obviously, $\text{Ag@AgCl}/\text{Bi}_2\text{O}_2\text{CO}_3$ nanocomposites show much smaller arc radii compared to $\text{Bi}_2\text{O}_2\text{CO}_3$. The reduced arc radius indicates a diminished resistance of working electrodes, suggesting a decrease in the solid state interface layer resistance and the charge transfer resistance across the solid-liquid junction on the surface by forming a heterojunction between Ag@AgCl and $\text{Bi}_2\text{O}_2\text{CO}_3$ [41]. Since the radius of the arc on the EIS spectra reflects the migration rate occurring at the surface, this suggests that a more effective separation of photo-generated electron-hole pairs and a faster interfacial charge transfer occurs on the $\text{Ag@AgCl}/\text{Bi}_2\text{O}_2\text{CO}_3$ surface under these conditions [42].

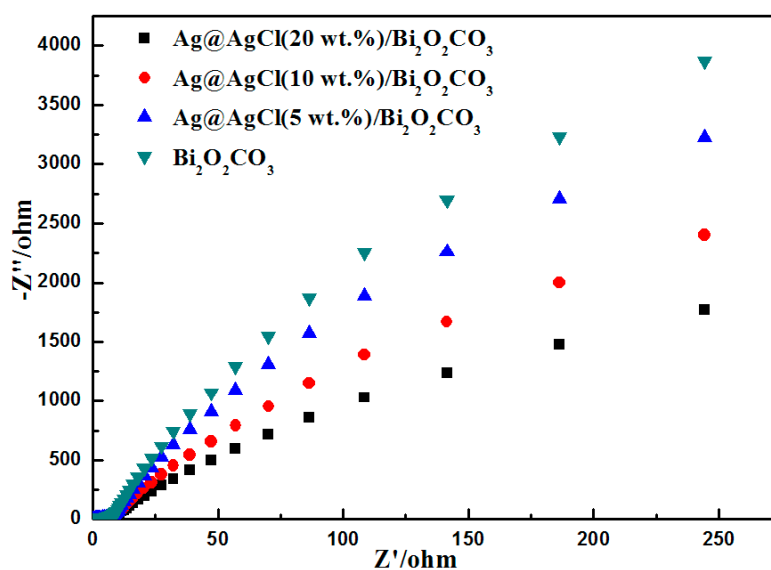


Figure 12. EIS spectra of synthesized $\text{Bi}_2\text{O}_2\text{CO}_3$, Ag@AgCl (5 wt %)/ $\text{Bi}_2\text{O}_2\text{CO}_3$, Ag@AgCl (10 wt %)/ $\text{Bi}_2\text{O}_2\text{CO}_3$ and Ag@AgCl (20 wt %)/ $\text{Bi}_2\text{O}_2\text{CO}_3$.

Bisphenol A (BPA) is a colorless organic compound and was chosen to further investigate and compare the photocatalytic activities of $\text{Ag@AgCl}/\text{Bi}_2\text{O}_2\text{CO}_3$ photocatalysts. Temporal changes in the concentration of BPA were monitored by examining the variation in maximal absorption in the UV-vis spectra at a wavelength of 275 nm. Figure 13a shows the photodegradation of BPA (C/C_0) over $\text{Ag@AgCl}/\text{Bi}_2\text{O}_2\text{CO}_3$ photocatalysts under visible light irradiation. The experimental results obtained indicate that the concentration of BPA was almost unchanged in the dark controls over 20 min, and that BPA molecules are very stable, experiencing almost no decomposition in the absence of a catalyst, which excludes the possibility of photolysis in the present system. The $\text{Ag@AgCl}/\text{Bi}_2\text{O}_2\text{CO}_3$ photocatalyst shows good photocatalytic activity for the degradation of BPA under visible light irradiation compared to $\text{Bi}_2\text{O}_2\text{CO}_3$ powders and Ag@AgCl photocatalysts. The total photocatalytic degradation of BPA over $\text{Ag@AgCl}/\text{Bi}_2\text{O}_2\text{CO}_3$, Ag@AgCl and $\text{Bi}_2\text{O}_2\text{CO}_3$ photocatalysts were 50.72%, 32.61% and 21.59%, respectively, after 20 min under visible light irradiation. The UV-vis spectral changes of BPA in aqueous solution over flower-like $\text{Ag@AgCl}/\text{Bi}_2\text{O}_2\text{CO}_3$ photocatalysts under visible light are plotted in Figure 13b as a function of irradiation time. This plot shows that the intensity of the maximum absorption peak of BPA at 275 nm decreases dramatically as visible light irradiation time increases within 20 min.

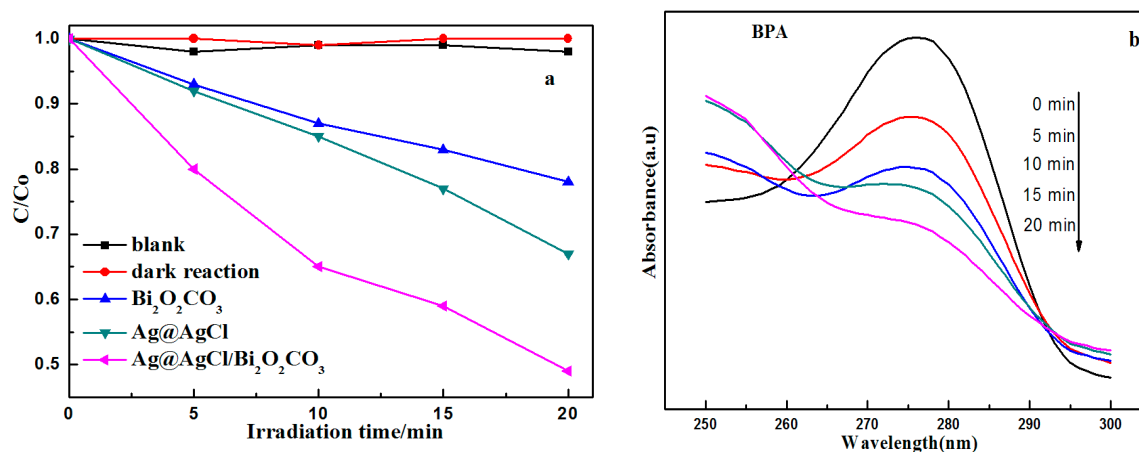


Figure 13. (a) Comparison of photocatalytic activities of the as-prepared samples for the photocatalytic degradation of BPA aqueous solutions; and (b) UV-vis spectral changes of BPA aqueous solutions in the presence of the $\text{Ag@AgCl/Bi}_2\text{O}_2\text{CO}_3$ sample under visible light irradiation.

Figure 14a shows the high performance liquid chromatography (HPLC) chromatogram during the photocatalytic degradation of BPA over Ag@AgCl (10 wt %)/ $\text{Bi}_2\text{O}_2\text{CO}_3$ under visible light irradiation. The BPA showed a characteristic peak at a retention time (RT) of 10.9 min. The BPA peak became weaker with increasing irradiation time, and the removal percent of BPA reached 51.4% within 20 min, indicating the excellent photocatalytic activity of Ag@AgCl (10 wt %)/ $\text{Bi}_2\text{O}_2\text{CO}_3$. Three-dimensional HPLC chromatography used to further demonstrate the photocatalytic activity of the Ag@AgCl (10 wt %)/ $\text{Bi}_2\text{O}_2\text{CO}_3$. As the degradation of organic pollutants BPA solution in the reaction of 0 min (Figure 14b) and 20 min (Figure 14c) shown, After 20 min illumination, the BPA corresponding peaks decrease, indicating that BPA was mineralized to CO_2 and H_2O in the process of photocatalytic reaction.

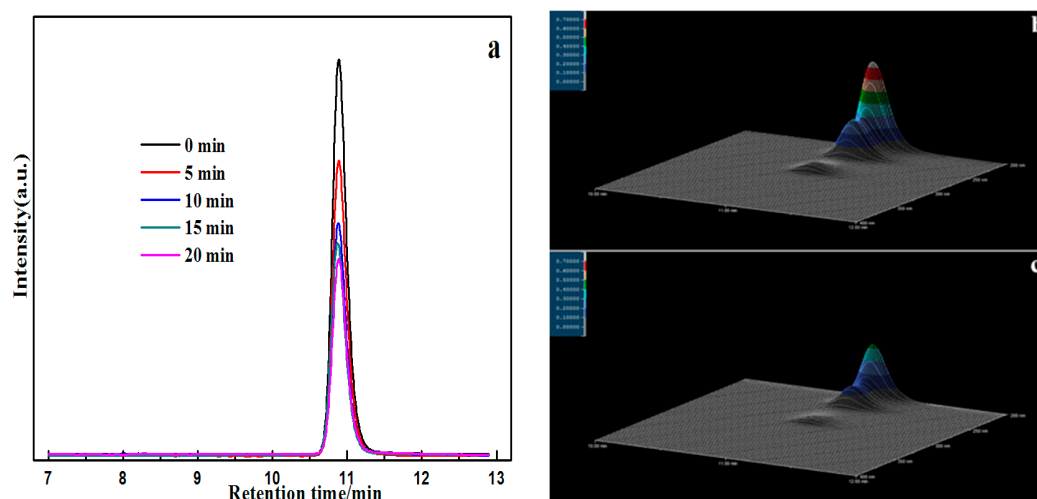


Figure 14. (a) HPLC chromatograms of BPA solutions with Ag@AgCl (10 wt %)/ $\text{Bi}_2\text{O}_2\text{CO}_3$ photocatalytic catalyst; (b) Three-dimensional HPLC chromatographic spectra of BPA degradation (0 min); (c) Three-dimensional HPLC chromatographic spectra of BPA degradation (30 min).

Combined with the above results, the $\text{Ag@AgCl/Bi}_2\text{O}_2\text{CO}_3$ composite photocatalyst showed a high photocatalytic activity for the photodegradation of MB dyes under visible light. The possible mechanisms for the enhancement of the photocatalytic activity of the $\text{Ag@AgCl/Bi}_2\text{O}_2\text{CO}_3$ composite photocatalyst are schematically illustrated in Figure 15. The surface plasmon resonance (SPR) of

Ag nanoparticles in the Ag@AgCl/Bi₂O₂CO₃ composite will additionally enhance visible light absorption. Under visible light irradiation, Ag NPs can be excited. Excited state Ag on the catalyst surface can transfer its photo-generated electrons to the CB of AgCl. On the basis of the relative position of the conduction band, the photo-generated electrons will transfer from the CB of AgCl (−0.95 eV) [43] to the CB of Bi₂O₂CO₃ (0.16 eV) [44], making an efficient charge separation and reducing the probability of electron–hole recombination. Simultaneously, the holes in the VB of Bi₂O₂CO₃ can transfer to AgCl, which causes the increased separation rate of photo-generated electrons and holes. The photo-generated holes on the surface of AgCl then react with Cl[−] to form Cl[•]. Cl[•] is a reactive radical species that oxidizes the surface-adsorbed organic pollutants, reducing the Cl[•] atoms back to Cl[−]. The resultant Cl[−] reacts with Ag⁺ to form AgCl again, maintaining the stability of the photocatalyst sample under visible light irradiation. While a portion of the holes on the VB of Ag could react with OH[−] or H₂O to form hydroxyl radicals (•OH), which have a strong oxidation ability to oxidize organic pollutant molecules, the holes could also oxidize the MB directly [45].

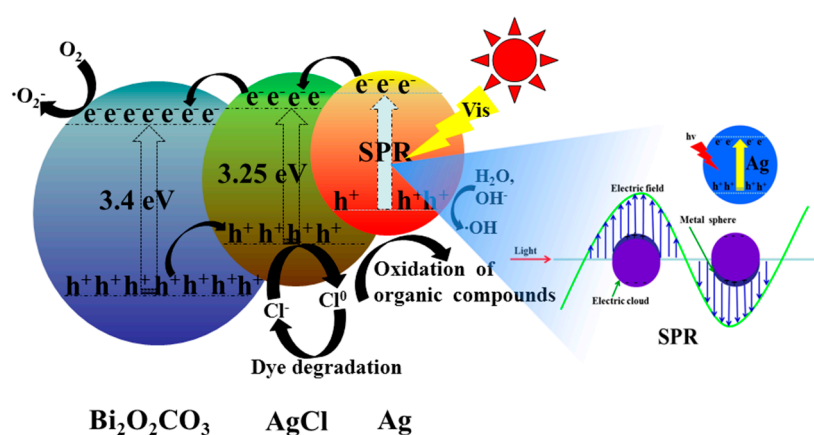


Figure 15. Mechanism of the photocatalytic degradation of MB over Ag@AgCl/Bi₂O₂CO₃.

4. Conclusions

In summary, a novel flower-like Ag@AgCl/Bi₂O₂CO₃ composite photocatalyst was synthesized by a facile oil-in-water self-assembly method. The introduction of Ag@AgCl nanoparticles into Bi₂O₂CO₃ was found to induce an increased photocatalytic activity under visible light irradiation. The formation of Ag@AgCl/Bi₂O₂CO₃ can improve the optical properties, the surface area, and charge transfer as well as hinder the recombination of electron–hole pairs, which is supposedly linked to the photocatalytic activity. Among the as-prepared samples, Ag@AgCl/Bi₂O₂CO₃ composites with 10 wt % Ag@AgCl showed the highest photocatalytic performances with regards to the degradation of organic pollutants. The photocatalyst also displayed higher stability during the photoreactions and no obvious deactivation was found for the recycled catalyst after five test runs. The present results suggest that hierarchical flower-like Ag@AgCl/Bi₂O₂CO₃ composites are a promising candidate for the photocatalytic degradation of organic dyes.

Acknowledgments: This work was funded by the National Natural Science Foundation of China (grant No. 51372068 and 21476161), Hebei Natural Science Funds for Distinguished Young Scholar (grant No. B2014209304), Key Program of Natural Science of Hebei Province (B2016209375), Hebei Provincial Foundation for International Cooperation (No. 15391403D) and National Science and Engineering Research Council of Canada (Discovery).

Author Contributions: For research articles with several authors, a short paragraph specifying their individual contributions must be provided. The following statements should be used “Shuanglong Lin and Zisheng Zhang conceived and designed the experiments; Shuanglong Lin and Li Liu performed the experiments; Shuanglong Lin and Wenquan Cui analyzed the data; Yinghua Liang contributed reagents/materials/analysis tools; Shuanglong Lin wrote the paper.” Authorship must be limited to those who have contributed substantially to the work reported.

Conflicts of Interest: The authors declare no conflict of interest.

References

1. Tang, J.W.; Zou, Z.G.; Ye, J.H. Efficient photocatalysis on BaBiO₃ driven by visible light. *J. Phys. Chem. C* **2007**, *111*, 12779–12785. [[CrossRef](#)]
2. Zhang, L.; Hashimoto, Y.; Taishi, T.; Nakamura, I.; Ni, Q.Q. Fabrication of flower-shaped Bi₂O₃ superstructure by a facile template-free process. *Appl. Surf. Sci.* **2011**, *257*, 6577–6582. [[CrossRef](#)]
3. Dumrongrojthanath, P.; Thongtem, T.; Phuruangrat, A.; Thongtem, S. Hydrothermal synthesis of Bi₂WO₆ hierarchical flowers with their photonic and photocatalytic properties. *Superlattice Microstruct.* **2013**, *54*, 71–77. [[CrossRef](#)]
4. Peng, S.J.; Li, L.L.; Zhu, P.N.; Wu, Y.Z.; Srinivasan, M.; Mhaisalkar, S.G.; Ramakrishna, S.; Yan, Q.Y. Controlled synthesis of BiOCl hierarchical self-assemblies with highly efficient photocatalytic properties. *Chem. Asian J.* **2013**, *8*, 258–268. [[CrossRef](#)] [[PubMed](#)]
5. Zhang, J.; Shi, F.J.; Lin, J.; Chen, D.F.; Gao, J.M.; Huang, Z.X.; Ding, X.X.; Tang, C.C. Self-assembled 3-D architectures of BiOBr as a visible lightdriven photocatalyst. *Chem. Mater.* **2008**, *20*, 2937–2941. [[CrossRef](#)]
6. Chen, R.; Cheng, G.; So, M.H.; Wu, J.L.; Lu, Z.; Che, C.M.; Sun, H.Z. Bismuth subcarbonate nanoparticles fabricated by water-in-oil microemulsionassisted hydrothermal process exhibit anti-Helicobacter pyloriproperties. *Mater. Res. Bull.* **2010**, *45*, 654–658. [[CrossRef](#)]
7. Hu, R.P.; Xiao, X.; Tu, S.H.; Zuo, X.X.; Nan, J.M. Synthesis of flower-like heterostructured β-Bi₂O₃/Bi₂O₂CO₃ microspheres using Bi₂O₂CO₃ self-sacrifice precursor and its visible-light-induced photocatalytic degradation of o-phenylphenol. *Appl. Catal. B* **2015**, *163*, 510–519. [[CrossRef](#)]
8. Dong, F.; Sun, Y.J.; Fu, M.; Ho, W.K.; Lee, S.C.; Wu, Z.B. Novel *in situ* N-doped (BiO)₂CO₃ hierarchical microspheres self-assembled by nanosheets as efficient and durable visible light driven photocatalyst. *Langmuir* **2012**, *28*, 766–773. [[CrossRef](#)] [[PubMed](#)]
9. Zhao, T.Y.; Zai, J.T.; Xu, M.; Zou, Q.; Su, Y.Z.; Wang, K.X.; Qian, X.F. Hierarchical Bi₂O₂CO₃ microspheres with improved visible-light-driven photocatalytic activity. *CrystEngComm* **2011**, *13*, 4010–4017. [[CrossRef](#)]
10. Madhusudan, P.; Yu, J.G.; Wang, W.G.; Cheng, B.; Liu, G. Facile synthesis of novel hierarchical grapheme-Bi₂O₂CO₃ composites with enhanced photocatalytic performance under visible light. *Dalton Trans.* **2012**, *41*, 14345–14353. [[CrossRef](#)] [[PubMed](#)]
11. Chen, L.; Huang, R.; Yin, S.F.; Luo, S.L.; Au, C.T. Flower-like Bi₂O₂CO₃: Facile synthesis and their photocatalytic application in treatment of dyecontaining wastewater. *Chem. Eng. J.* **2012**, *193–194*, 123–130. [[CrossRef](#)]
12. Cao, X.F.; Zhang, L.; Chen, X.T.; Xue, Z.L. Persimmon-like (BiO)₂CO₃ microstructures: Hydrothermal preparation, photocatalytic properties and their conversion into Bi₂S₃. *CrystEngComm* **2011**, *13*, 1939–1945. [[CrossRef](#)]
13. Liu, Y.Y.; Wang, Z.Y.; Huang, B.B.; Yang, K.S.; Zhang, X.Y.; Qin, X.Y.; Dai, Y. Preparation, electronic structure, and photocatalytic properties of Bi₂O₂CO₃ nanosheet. *Appl. Surf. Sci.* **2010**, *257*, 172–175. [[CrossRef](#)]
14. Zheng, Y.; Duan, F.; Chen, M.Q.; Xie, Y. Synthetic Bi₂O₂CO₃ nanostructures: Novel photocatalyst with controlled special surface exposed. *J. Mol. Catal. A Chem.* **2010**, *317*, 34–40. [[CrossRef](#)]
15. Cheng, H.F.; Huang, B.B.; Yang, K.S.; Wang, Z.Y.; Qin, X.Y.; Zhang, X.Y.; Dai, Y. Facile template-free synthesis of Bi₂O₂CO₃ hierarchical microflowers and their associated photocatalytic activity. *Chemphyschem* **2010**, *11*, 2167–2173. [[CrossRef](#)] [[PubMed](#)]
16. Yu, L.H.; Zhang, X.Y.; Li, G.W.; Cao, Y.T.; Shao, Y.; Li, D.Z. Highly efficient Bi₂O₂CO₃/BiOCl photocatalyst based on heterojunction with enhanced dye-sensitization under visible light. *Appl. Catal. B* **2016**, *187*, 301–309. [[CrossRef](#)]
17. Kowalska, E.; Remita, H.; Colbeau-Justin, C.; Hupka, J.; Belloni, J. Modification of titanium dioxide with platinum ions and clusters: Application in photocatalysis. *J. Phys. Chem. C* **2008**, *112*, 1124–1131. [[CrossRef](#)]
18. Wang, Q.Z.; Yun, G.X.; Bai, Y.; An, N.; Lian, J.H.; Huang, H.H.; Su, B.T. Photodegradation of rhodamine B with MoS₂/Bi₂O₂CO₃ composites under UV light irradiation. *Appl. Surf. Sci.* **2014**, *313*, 537–544. [[CrossRef](#)]
19. Tian, N.; Huang, H.W.; Guo, Y.X.; He, Y.; Zhang, Y.H. A g-C₃N₄/Bi₂O₂CO₃ composite with high visible-light-driven photocatalytic activity for rhodamine B degradation. *Appl. Surf. Sci.* **2014**, *322*, 249–254. [[CrossRef](#)]

20. Hu, D.D.; Zhang, K.Y.; Yang, Q.; Wang, M.J.; Xi, Y.; Hu, C.G. Super-high photocatalytic activity of Fe₂O₃ nanoparticles anchored on Bi₂O₂CO₃ nanosheets with exposed {0 0 1} active facets. *Appl. Surf. Sci.* **2014**, *316*, 93–101. [[CrossRef](#)]
21. Jin, L.; Zhu, G.Q.; Hojamberdiev, M.; Luo, X.C.; Tan, C.W.; Peng, J.H.; Wei, X.M.; Li, J.P.; Liu, P. A Plasmonic Ag–AgBr/Bi₂O₂CO₃ Composite Photocatalyst with Enhanced Visible-Light Photocatalytic Activity. *Ind. Eng. Chem. Res.* **2014**, *35*, 13718–13727. [[CrossRef](#)]
22. Zhang, L.S.; Wong, K.H.; Chen, Z.G.; Yu, J.C.; Zhao, J.C.; Hu, C.; Chang, C.Y.; Wong, P.K. AgBr–Ag–Bi₂WO₆ nanojunction system: A novel and efficient photocatalyst with double visible-light active components. *Appl. Catal. A* **2009**, *363*, 221–229. [[CrossRef](#)]
23. Hu, X.X.; Hu, C.; Peng, T.W.; Zhou, X.F.; Qu, J.H. Plasmon-induced inactivation of enteric pathogenic microorganisms with Ag–AgI/Al₂O₃ under visible-light irradiation. *Environ. Sci. Technol.* **2010**, *44*, 7058–7062. [[CrossRef](#)] [[PubMed](#)]
24. Dong, F.; Li, Q.Y.; Zhou, Y.; Sun, Y.J.; Zhang, H.D.; Wu, Z.B. *In situ* decoration of plasmonic Ag nanocrystals on the surface of (BiO)₂CO₃ hierarchical microspheres for enhanced visible light photocatalysis. *Dalton Trans.* **2014**, *43*, 9468–9480. [[CrossRef](#)] [[PubMed](#)]
25. Peng, S.J.; Li, L.L.; Tan, H.T.; Wu, Y.Z.; Cai, R.; Yu, H.; Huang, X.; Zhu, P.N.; Ramakrishna, S.; Srinivasana, M.; *et al.* Monodispersed Ag nanoparticles loaded on the PVP-assisted synthetic Bi₂O₂CO₃ microspheres with enhanced photocatalytic and supercapacitive performances. *J. Mater. Chem. A* **2013**, *1*, 7630–7638. [[CrossRef](#)]
26. Yu, J.C.; Yu, J.G.; Ho, W.K.; Jiang, Z.T.; Zhang, L.Z. Effects of F-doping on the photocatalytic activity and microstructures of nanocrystalline TiO₂ powders. *Chem. Mater.* **2002**, *14*, 3808–3816. [[CrossRef](#)]
27. Wang, Q.Z.; Zheng, L.H.; Chen, Y.T.; Fan, J.F.; Huang, H.H.; Su, B.T. Synthesis and characterization of novel PPy/Bi₂O₂CO₃ composite with improved photocatalytic activity for degradation of Rhodamine-B. *J. Alloys Compd.* **2015**, *637*, 127–132. [[CrossRef](#)]
28. Huang, H.W.; Wang, S.B.; Tian, N.; Zhang, Y.H. One-step hydrothermal preparation strategy for layered BiO₄/Bi₂WO₆ heterojunctions with enhanced visible light photocatalytic activities. *RSC Adv.* **2014**, *4*, 5561–5567. [[CrossRef](#)]
29. He, Y.M.; Cai, J.; Zhang, L.H.; Wang, X.X.; Lin, H.J.; Teng, B.T.; Zhao, L.H.; Weng, W.Z.; Wan, H.L.; Fan, M.H. Comparing two new composite photocatalysts, t-LaVO₄/g-C₃N₄ and m-LaVO₄/g-C₃N₄, for their structures and performances. *Ind. Eng. Chem. Res.* **2014**, *53*, 5905–5915. [[CrossRef](#)]
30. Huang, H.W.; Yao, J.Y.; Lin, Z.S.; Wang, X.Y.; He, R.; Yao, W.J.; Zhai, N.X.; Chen, C.T. NaSr₃Be₃B₃O₉F₄: A promising deep-ultraviolet nonlinear optical material resulting from the cooperative alignment of the [Be₃B₃O₁₂F]¹⁰⁻ anionic group. *Angew. Chem. Int. Ed.* **2011**, *50*, 9141–9144. [[CrossRef](#)] [[PubMed](#)]
31. Yu, J.G.; Yu, H.G.; Cheng, B.; Zhao, X.J.; Yu, J.C.; Ho, W.K. The effects of calcination temperature on the surface microstructure and photocatalytic activity of TiO₂ thin films prepared by liquid phase deposition. *J. Phys. Chem. B* **2003**, *107*, 13871–13879. [[CrossRef](#)]
32. Ao, Y.H.; Xu, L.Y.; Wang, P.F.; Wang, C.; Hou, J.; Qian, J. Preparation of CdS nanoparticle loaded flower-like Bi₂O₂CO₃ heterojunction photocatalysts with enhanced visible light photocatalytic activity. *Dalton Trans.* **2015**, *44*, 11321–11330. [[CrossRef](#)] [[PubMed](#)]
33. Zhuang, J.D.; Dai, W.X.; Tian, Q.F.; Li, Z.H.; Xie, L.Y.; Wang, J.X.; Liu, P. Photocatalytic degradation of RhB over TiO₂ bilayer films: Effect of defects and their location. *Langmuir* **2010**, *26*, 9686–9694. [[CrossRef](#)] [[PubMed](#)]
34. Sun, D.F.; Han, Y.D.; Gao, S.; Zhang, X.L. Surface modification of titania-coated cobalt ferrite magnetic photocatalyst by cold plasma. *Surf. Coat. Technol.* **2013**, *228*, 516–519. [[CrossRef](#)]
35. Li, W.J.; Li, D.Z.; Wang, J.X.; Shao, Y.; You, J.M.; Teng, F. Exploration of the active species in the photocatalytic degradation of methyl orange under UV light irradiation. *J. Mol. Catal. A Chem.* **2013**, *380*, 10–17. [[CrossRef](#)]
36. Cao, J.; Xu, B.Y.; Lin, H.L.; Luo, B.D.; Chen, S.F. Chemical etching preparation of BiOI/BiOBr heterostructures with enhanced photocatalytic properties for organic dye removal. *Chem. Eng. J.* **2012**, *185–186*, 91–99. [[CrossRef](#)]
37. Zhou, Z.J.; Long, M.C.; Cai, W.M.; Cai, J. Synthesis and photocatalytic performance of the efficient visible light photocatalyst Ag–AgCl/BiVO₄. *J. Mol. Catal. A Chem.* **2012**, *353–354*, 22–28. [[CrossRef](#)]
38. Xu, Y.G.; Xu, H.; Yan, J.; Li, H.M.; Huang, L.Y.; Xi, J.X.; Yin, S.; Shu, H.M. A plasmonic photocatalyst of Ag/AgBr nanoparticles coupled with g-C₃N₄ with enhanced visible-light photocatalytic ability. *Colloids Surf. A* **2013**, *436*, 474–483. [[CrossRef](#)]

39. Huang, H.W.; Li, X.W.; Wang, J.J.; Dong, F.; Chu, P.K.; Zhang, T.R.; Zhang, Y.H. Anionic group self-doping as a promising strategy: Band-gap engineering and multi-functional applications of high-performance CO_3^{2-} -doped $\text{Bi}_2\text{O}_2\text{CO}_3$. *ACS Catal.* **2015**, *5*, 4094–4103. [[CrossRef](#)]
40. Zhang, Q.; Wang, H.Y.; Hu, S.Z.; Lu, G.; Bai, J.; Kang, X.X.; Liu, D.; Gui, J.Z. Synthesis and properties of visible light responsive g- $\text{C}_3\text{N}_4/\text{Bi}_2\text{O}_2\text{CO}_3$ layered heterojunction nanocomposites. *RSC Adv.* **2015**, *5*, 42736–42743. [[CrossRef](#)]
41. He, B.L.; Dong, B.; Li, H.L. Preparation and electrochemical properties of Ag-modified TiO_2 nanotube anode material for lithium-ion battery. *Electrochem. Commun.* **2007**, *9*, 425–430. [[CrossRef](#)]
42. Huang, Q.W.; Tian, S.Q.; Zeng, D.W.; Wang, X.X.; Song, W.L.; Li, Y.Y.; Xiao, W.; Xie, C.S. Enhanced photocatalytic activity of chemically bonded TiO_2 /graphene composites based on the effective interfacial charge transfer through the C-Ti bond. *ACS Catal.* **2013**, *3*, 1477–1485. [[CrossRef](#)]
43. Liang, Y.H.; Lin, S.L.; Hu, J.S.; Liu, L.; McEvoy, J.G.; Cui, W.Q. Facile hydrothermal synthesis of nanocomposite $\text{Ag@AgCl}/\text{K}_2\text{Ti}_4\text{O}_9$ and photocatalytic degradation under visible light irradiation. *J. Mol. Catal. A Chem.* **2014**, *383–384*, 231–238. [[CrossRef](#)]
44. Chen, L.; Yin, S.F.; Luo, S.L.; Huang, R.; Zhang, Q.; Hong, T.; Au, P.C.T. $\text{Bi}_2\text{O}_2\text{CO}_3/\text{BiOI}$ photocatalysts with heterojunctions highly efficient for visible-light treatment of dye-containing wastewater. *Ind. Eng. Chem. Res.* **2012**, *51*, 6760–6768. [[CrossRef](#)]
45. Hu, C.; Lan, Y.Q.; Qu, J.H.; Hu, X.X.; Wang, A.M. Ag/AgBr/ TiO_2 visible light photocatalyst for destruction of azodyes and bacteria. *J. Phys. Chem. B* **2006**, *110*, 4066–4072. [[CrossRef](#)] [[PubMed](#)]



© 2016 by the authors; licensee MDPI, Basel, Switzerland. This article is an open access article distributed under the terms and conditions of the Creative Commons Attribution (CC-BY) license (<http://creativecommons.org/licenses/by/4.0/>).